Thin Solid Films, *237* (1994) 225–230

Scanning tunneling microscopy imaging of conducting Langmuir–Blodgett films

Marcello Mulè, Elisa Stussi and Danilo de Rossi
Centro 'E. Piaggio', University of Pisa, via Diotisalvi 2, I-56126 Pisa (Italy)

Tatiana S. Berzina and Vladimir I. Troitsky
Zelenograd Research Institute of Physical Problems, 103460 Moscow (Russian Federation)

(Received November 26, 1992; revised March 25, 1993; accepted July 2, 1993)

Abstract

Atomic resolution imaging of Langmuir–Blodgett highly-conductive, environmentally-stable organic films of charge-transfer salts has been obtained by scanning tunnelling microscopy (STM) showing their closely packed structure. By means of a comparative study with images of highly oriented pyrolytic graphite, the intermolecular distances have been calculated taking into account several types of measurement error. The structural data derived from STM have been compared with those obtained from electron diffraction studies. The electrical properties of these films together with the "read and write" capabilities of STM could provide a basis for fabricating nanoelectronic devices.

1. Introduction

Langmuir–Blodgett (LB) ordered organic monolayers and multilayers have been a subject of growing interest in the last few years because of their peculiar properties and because of their possible application in the field of molecular electronics [1]. Despite the various studies which have been carried out, there are still considerable objective difficulties in obtaining exact molecular information about these films because of the limited efficacy of traditional characterization techniques such as scanning electron microscopy (SEM) and electron diffraction. Among the new investigation methods, scanning tunnelling microscopy (STM) [2] and atomic force microscopy (AFM) [3] have proved to be effective for providing atomic resolution imaging of LB films, as shown by the large amount of published work. In comparison with transmission electron microscopy (TEM), STM and AFM present the advantage of operating in air, requiring little sample preparation, and being potentially non-destructive methods.

However, only LB films of one or two insulating monolayers on a conductive substrate have been studied by STM techniques [4–10], while quite extensive studies have been carried out on charge-transfer salt (CTS) crystals, obtained by electrocrystallization or precipitation, using the STM technique [11–15].

We report here an STM study of conductive organic LB films of CTS, up to 20 monolayers, deposited on highly oriented pyrolytic graphite (HOPG). LB films of such type based on the charge-transfer salt of TCNQ with octodecylpyridinium were first deposited several years ago by Ruaudel-Teixier *et al.* [16]. Conducting LB films of many other compounds were obtained later [17–19]. Conductivity of the mentioned LB films is strongly anisotropic. They consist of super thin conducting planes separated by insulating regions of hydrocarbon chains, therefore, the films are supposed to be conducting in the layer plane and insulating in the normal direction. Despite this fact, atomic resolution images were recorded for thick LB films in our experiments. Quantitative measurements of intermolecular distances for the upper layer of the film were carried out adopting a set of remedies that reduce errors, and some parameters of the unit cell were determined. A good correlation between STM data and quantitative data obtained from electron diffraction patterns has been found.

2. Experimental details

The procedure for forming the conducting LB films of CTS used in this present work was based on the interaction between surfactant donor molecules of hexadecylbis(ethylenedithio)tetrathiafulvalene (C_{16}-BEDT-TTF) spread at the air–water interface and inorganic compounds ($FeCl_3$) dissolved in water. In order to increase the stability of the monolayers of C_{16}-BEDT-TTF at the air–water interface, acceptor molecules of heptadecyl-

0040-6090/94/$7.00

TABLE 1. Deposition parameters

Spreading solvents	Hexane–chloroform 2:1 in volume
Concentration of compound	0.33 mg ml^{-1}
Surface pressure	18–25 mN m^{-1}
Subphase	10^{-4} M $FeCl_3$ in MilliQ water
Temperature	20 °C
pH of subphase	3.8
Number of monolayers	10–15–20

oxycarbonyltetracyanoanthraquinodimethane ($C_{17}H_{35}$-OC-TCNAQ), were mixed in the molar ratio 1:10 with donor molecules. In fact a parallel study [20], in which this mixture has been investigated, has proved that a small amount of acceptor molecules stabilizes the monolayer without appreciably changing the electrical properties of the deposited films. In terms of conductivity and mechanical stability of the monolayer, the optimum is achieved using a donor–acceptor molar ratio of 10:1. All deposition parameters are reported in Table 1.

Films of 20 monolayers, obtained according to this procedure, showed a conductivity of about 2 Ω^{-1} cm^{-1} in a direction parallel to the film. Further details about film spreading conditions and macroscopic characterization are available in ref. 20.

Donor and acceptor molecules consist of hydrophobic tails about 2.0 nm long and of polar heads which are responsible for conduction. In order to investigate these multilayers by STM, several monolayers have been deposited on HOPG (hydrophobic), which is commonly used in STM because of its high conductivity and atomic flatness on relative large areas.

A commercial LB Trough (Lauda Filmwaage, Königshofen, Germany) has been utilized for deposition. The deposition on HOPG substrates by the vertical lift technique was found to be impossible. For this reason the horizontal lift technique [21] was used, but, as a result, the X-type polar structure was not obtained: in fact, a rearrangment of the monolayer occurs during each transfer action, and the Y-type non-polar structure is obtained. This configuration is confirmed by contact angle measurements, showing that the sample is hydrophobic after every touching of the subphase surface covered by the compressed monolayer during film deposition. Details of the deposition process are shown in Fig. 1. If the monolayer is liquid ("two-dimensional" liquid crystal) as in this case, barrier feedback can compress the monolayer after each successive touching of the surface, and the process proceeds as shown in Fig. 1. In the ideal case exactly two monolayers are transferred (transfer ratio, 2). Unfortunately, if such a technique is used in this case feedback occurs very quickly after withdrawing the substrate, and, as a rule, collapse of the monolayer takes place. For this reason the horiontal lift technique was adopted, using a special

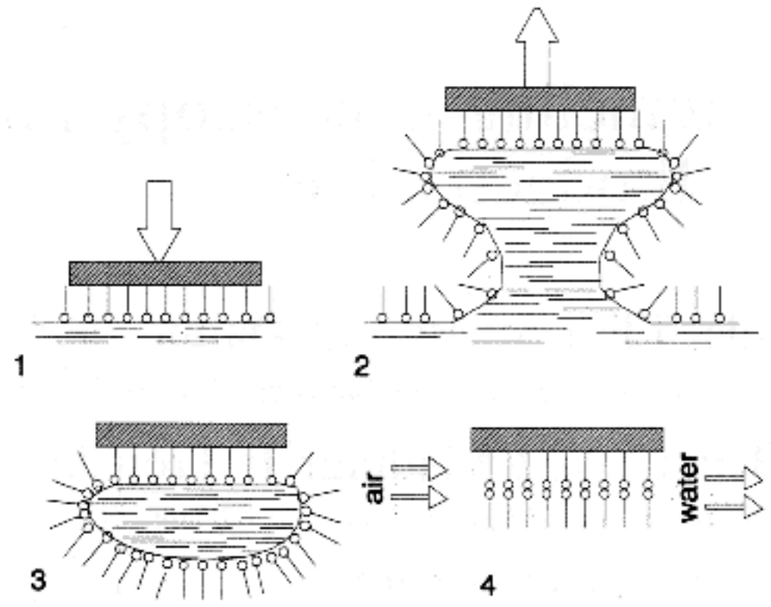

Fig. 1. Scheme of LB film deposition via the horizontal lift technique with operating feedback.

grid for sectioning the monolayer (as in the case of solid monolayers) and switching off the feedback when the desired pressure was reached. The character of monolayer reconstruction is really the same as shown above. However, the transfer ratio is less than 2, but greater than 1. Such a situation occurs when, after each act of transfer, multiple microscopic areas are not covered by the bilayer; however, the sample surface always remains hydrophobic, since the substrate was initially hydrophobic and any area covered by a bilayer is hydrophobic as well. Fortunately, a rather uniform LB film is deposited for the compound used, *i.e.* the defect density does not, in practice, increase with film thickness. For this reason, it can be argued that every new bilayer crystallizes preferentially on the areas which are not covered by the previous bilayer.

A commercial STM Park Scientific Instrument (USA) has been used, operating in air at room temperature, on an antivibration table, and connected to a PC-486 33 MHz, in which image acquisition and the visualization program are run in a WINDOWS 3.1 environment. The data acquired are stored in a matrix of 256 × 256 elements.

The microscope tungsten tips are obtained by electrochemical etching: a 0.5 mm diameter tungsten wire is dipped in a NaOH 1 M solution and an a.c. voltage of about 30 V is applied between the wire and the platinum counterelectrode in the solution until the tip is formed.

Data acquisition was carried out in the current imaging mode (constant height). This permits the avoidance of the instrument feedback which generates noise and limits the scanning speed because of its low pass filter. A high scanning speed is necessary, as will be seen hereinafter, in order to reduce thermal drift effects that are considerable on an atomic scale. On the other hand, when working in the current imaging mode quantitative information concerning roughness profiles in a direction normal to the substrate is lost. A variable tunnel

voltage of 0.1–0.5 V and a mean current value of 100 pA were used. In fact, in the current imaging mode, differing from the constant height mode, the instantaneous current is obviously not constant because the instrument feedback is inactivated. However, its mean value is kept constant (at 100 pA in our case) by a slow instrument feedback that is essential for compensating thermal effects.

Because of an unavoidable small tilt between tip scanning plane and sample surface, many images appear to have a different level of luminosity linearly changing from one side to the other. The same effect can be caused by changes in conductivity, but in such a case, the change in luminosity should appear more irregular. This effect prevents the achievement of a contrast sufficient enough to resolve the molecular pattern in all the images viewed. This problem has been solved calculating and subtracting the interpolating plane of each image by means of a purposely written software routine. The removal of the interpolating plane has been the only image processing carried out. Acquisitions were repeated on the same samples after one month and no change in the molecular structure of the film was observed.

In order to exactly characterize the film on an atomic scale, *i.e.* to record the pattern and to determine the intermolecular distances, several strategies have been adopted which remove or reduce those errors that can affect the measurement on an atomic scale. The principal sources of noise will be now illustrated, together with the adopted remedies. Thermal drifts are probably the most visible disturbance during data acquisition. In order to reduce this effect we operated with the maximum line scanning frequency allowed by our scanning tunnelling microscope, *i.e.* 80 Hz. In fact, the shorter the total time for the acquisition of an image, the smaller the horizontal relative displacement between tip and sample due to thermal effects becomes. Every image acquired at such a frequency was always followed by another acquired at 40 Hz, in order to evaluate the amount of thermal drift. A good correspondence between the images obtained in almost every tandem acquisition confirmed that a 80 Hz frequency is high enough to make thermal effects insignificant.

Given that the sensitivity of the piezoelectric transducer along the directions parallel to the sample is dependent on its average elongation, it was always necessary to operate with a constant elongation value.

Other sources of error arose from a different sensitivity between the two directions parallel to the sample and to the impossibility of setting the absolute scanning dimensions exactly. In fact, when images were acquired at the molecular level, the absolute error in the scanning area set-up was of the same order of magnitude as the dimensions of the scanning area itself. Both types of error were reduced using the following procedure.

Uncharted HOPG images on an atomic scale are acquired with changing scanning dimensions until a regular hexagonal pattern is obtained, *i.e.* the well-known HOPG structure.

LB film images are successively acquired with minimum delay without changing scanning dimensions.

Returning to uncoated HOPG, the hexagonal pattern is checked again.

The true scanning dimensions are deduced by comparison with uncoated HOPG images, whose dimensions are well known from the literature [22].

The dimensions on LB film images are deduced by comparison with uncoated HOPG images.

The visible distortion on the left side of every image may be caused by the non-linear behaviour of the piezo-tube near the point of scan reversal. The area in which this distortion is present must be excluded for film dimension calculation. Stochastic errors have been reduced by averaging the measurement of dimensions on several images.

Deposition of the films for electron diffraction studies was made on copper grids with meshes of about 0.1 mm coated with a collodion film 10–20 nm thick. Electron diffraction patterns were obtained using the equipment described in ref. 23 and spacings were determined accordingly.

3. Results and discussion

An image of uncoated HOPG is shown in Fig. 2, the distances between atoms being reported on the right. The typical hexagonal pattern is clearly visible.

Figure 3(a) shows a typical image of our charge-transfer salts film and Fig. 4 shows an image acquired on the same sample, one month later: molecules are arranged regularly, showing the closely packed structure. In accordance with the patterns obtained, the unit cell can be monoclinic or triclinic. Some vectors of the crystalline lattice parameters a, b and g of the unit cell are indicated in Fig. 3(b). The mean values of the distances between the spots in STM images, calculated using a set of 20 patterns, are reported, together with their variances, in Table 2.

As can be seen from the Table, there is little dispersion of data. No correlation has been found between distances in the images and the number of deposited monolayers, scanning frequency or subphase molarity. The possibility that the HOPG pattern could affect film configuration is unlikely because of the high number of deposited monolayers (up to 20).

If the r_1 and r_2 distances in the STM image are chosen as the a and b parameters of the unit cell an area per molecule A will be equal to:

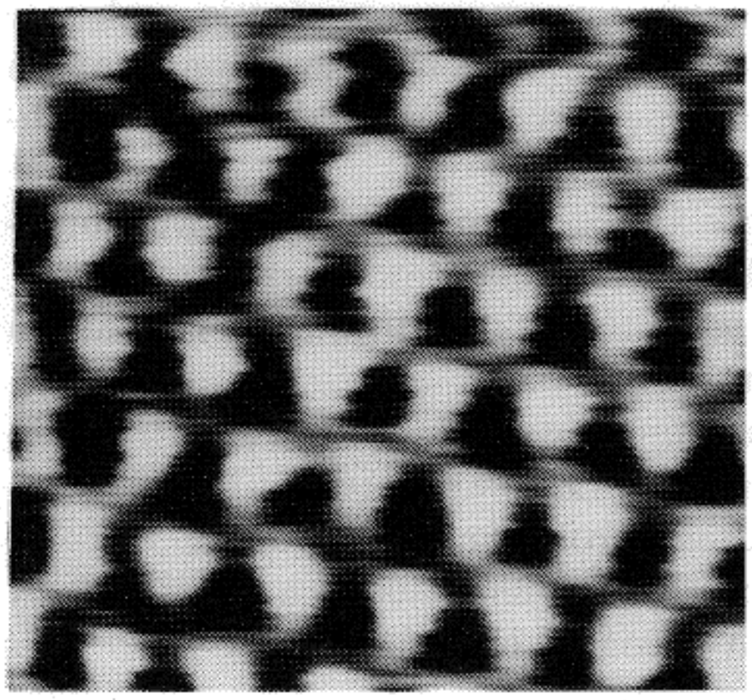

Fig. 2. High resolution STM image of HOPG.

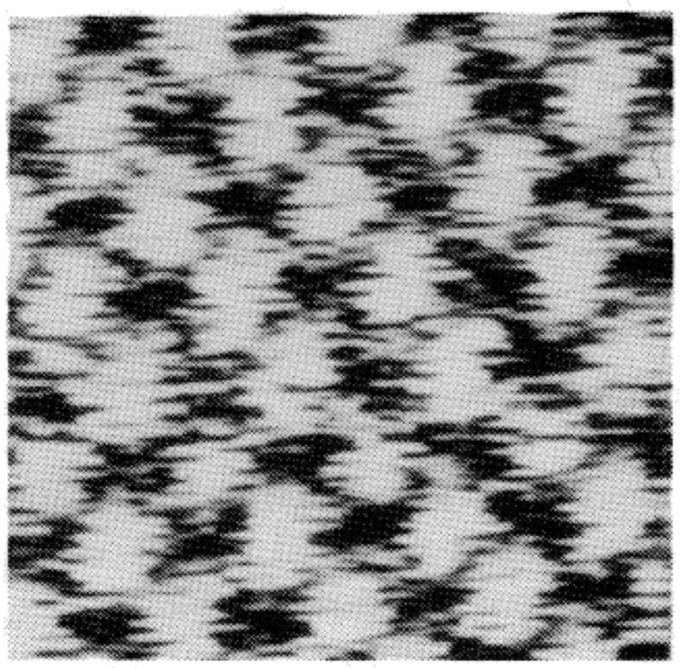

(a)

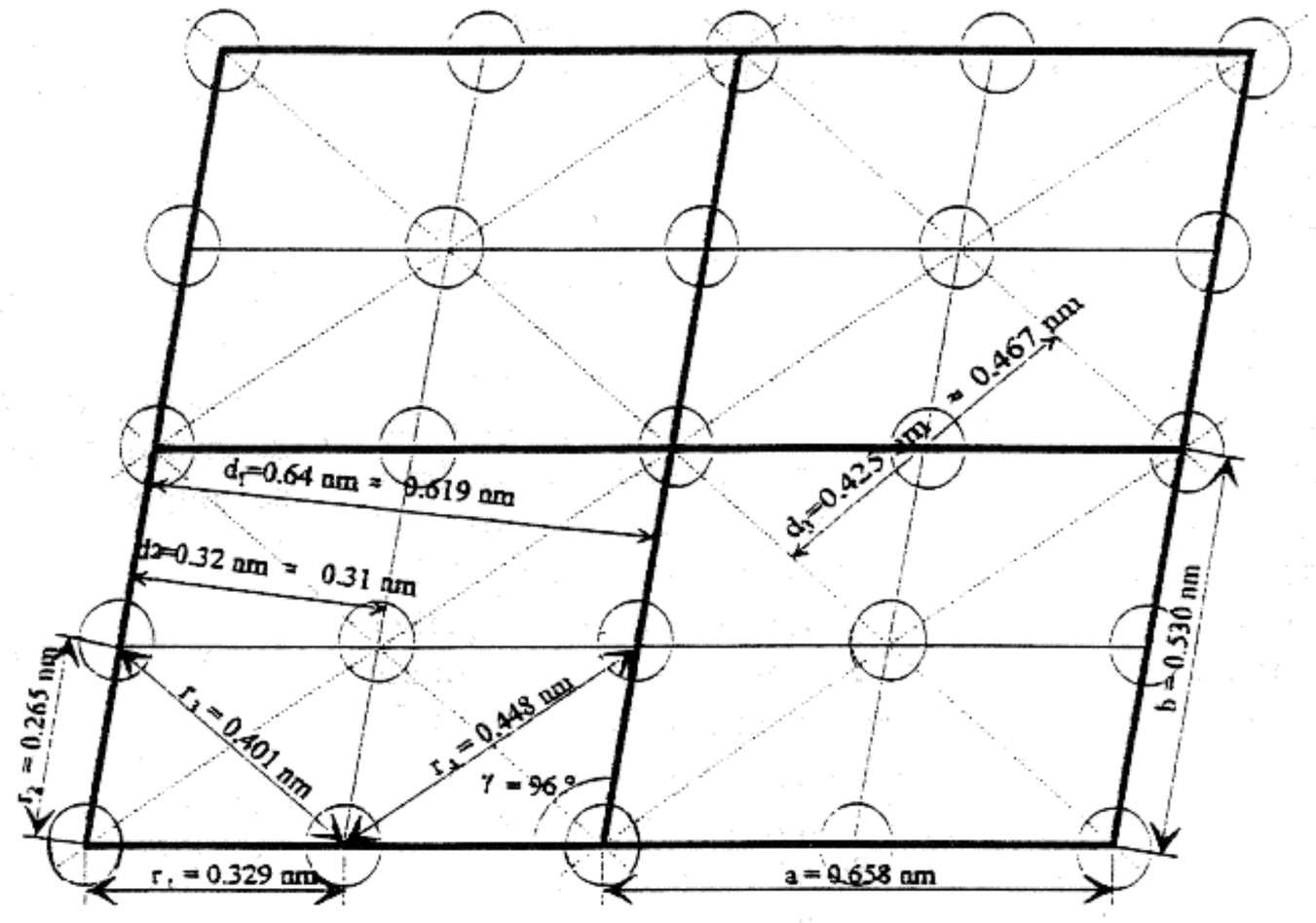

(b)

Fig. 3. High resolution STM image of LB films (a) and the suggested unit cell (b) (circles correspond to white spots on CTS STM images).

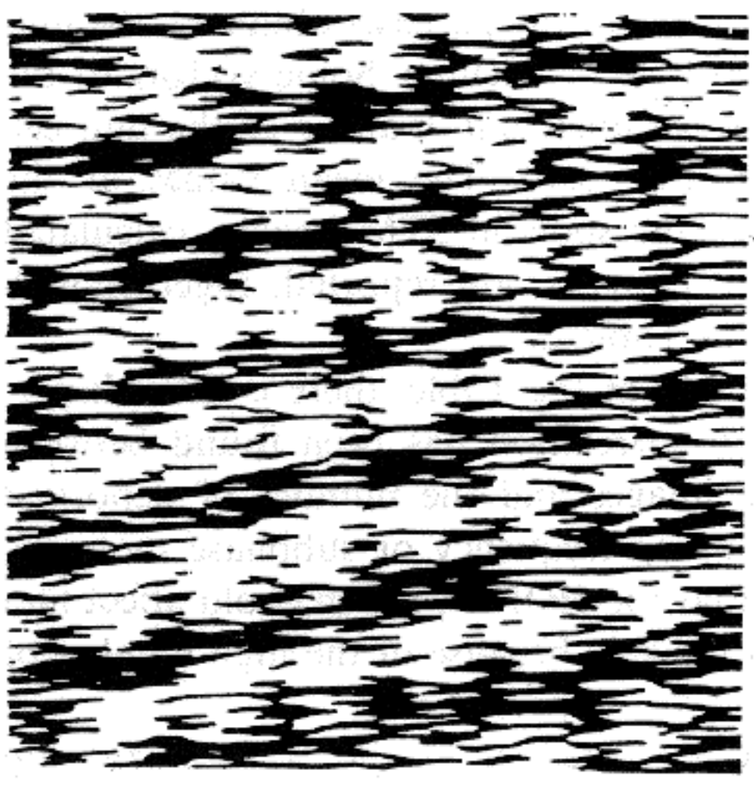

Fig. 4. STM image acquired on the same sample as Fig. 3, one month later.

TABLE 2. Values of parameters measured—in the STM image of the LB film

	r_1 (nm)	r_2 (nm)	r_3 (nm)	r_4 (nm)	γ (deg)
Average	0.329	0.265	0.401	0.448	95.99
Variance	0.019	0.009	0.013	0.026	3.91

$$A = r_1 r_2 \sin(\gamma) = 0.0867 \text{ nm}^2$$

which is unrealistic.

On the other hand, the area per molecule of C_{16}-BEDT-TTF is measured [20] to be of the order of 0.35 nm^2 which is, with a good approximation, four times the value of A. Thus, the real parameters of the unit cell can be: a, 0.658 nm; b, 0.530 nm; γ, 96.0°. From electron diffraction data d_1, d_2 and d_3 spacings

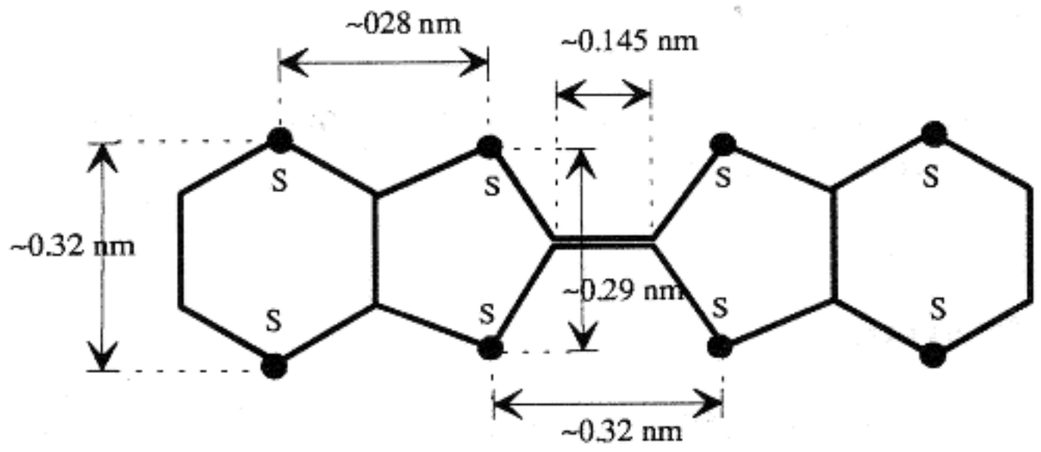

Fig. 5. The C_{16}-BEDT-TTF head.

(see Fig. 3(b)) have been found to be 0.619, 0.310 and 0.467 nm respectively, showing a good correspondence with the STM findings.

Referring to Fig. 5, in which the structure of the C_{16}-BEDT-TTF polar head is shown, it can be noticed that relevant distances among sulphur atoms are very close to r_1 and r_2. This additional observation leads us to suggest that bright spots in the STM images may correspond to sulphur atoms. A possible model supporting this hypothesis is shown in Fig. 6: sulphur atoms of BEDT-TTF fragments located near the contact plane of two adjacent monolayers (ringed with dotted curves) are supposed to decrease their electron density due to charge transfer to ferrous ions disposed on the contact area. These groups of atoms could therefore be a target for electron tunnelling. In addition, molecules of adjacent monolayers are supposed to be connected to each other by glide planes. The angle between the layer plane and the axis of BEDT-TTF fragments, roughly evaluated on the basis of the close packing of the latter, is also indicated in Fig. 6.

On the other hand, the proposed model is just one of the many possible, since very little is known about the film structure. In fact, structure analysis is impossible because only three reflections (two independent) appear in the electron diffraction pattern; thus, practically an infinite number of molecular packing patterns is possible for the determined unit cell. In addition, nothing is known on the electron density distribution in BEDT-TTF groups caused by charge transfer to ferrous ions: simply because of this distribution specific zones in the molecule can arise, which are the targets of electron tunnelling. Several other reasons of uncertainty can arise, and even the proposed model can be in some contradiction with the principle of close packing for a molecular crystal, as can be understood by comparing Fig. 3 with Fig. 6. In conclusion, the major problem is that no detailed interpretation is possible in the absence of sufficient experimental structural data, since the interpretation of STM data is not yet developed to such an extent as that of X-ray or electron diffraction. A few additional considerations are now made regarding a possible scheme of the tunnelling electron paths during STM imaging, as depicted schematically in Fig. 7. As already mentioned in this paper, it may be argued that, after rearrangement of the film, the insulating hydrocarbon tails (approximately 2 nm long) of C_{16}-BEDT-TTF constitute the uppermost layer of the film coming in contact with the STM tip during image formation. In order for electron tunnelling to occur into the first conducting layer of the C_{16}-BEDT-TTF heads, a partial penetration of the tip into the insulating first layer has to be assumed, or the insulating tails can be supposed to be tilted with respect to the normal to the layer plane. Moreover, proceeding from the real area per molecule and the necessity of close packing of the hydrocarbon chains, tilt angles of the latter can be evaluated because their cross-section is approximately equal to 0.2 nm^2. Thus, hydrocarbon chains are tilted by an angle of at least 50°. The latter case is more probable, since stable STM images have been obtained with high reproducibility when different scanning speeds and directions were used and even when the

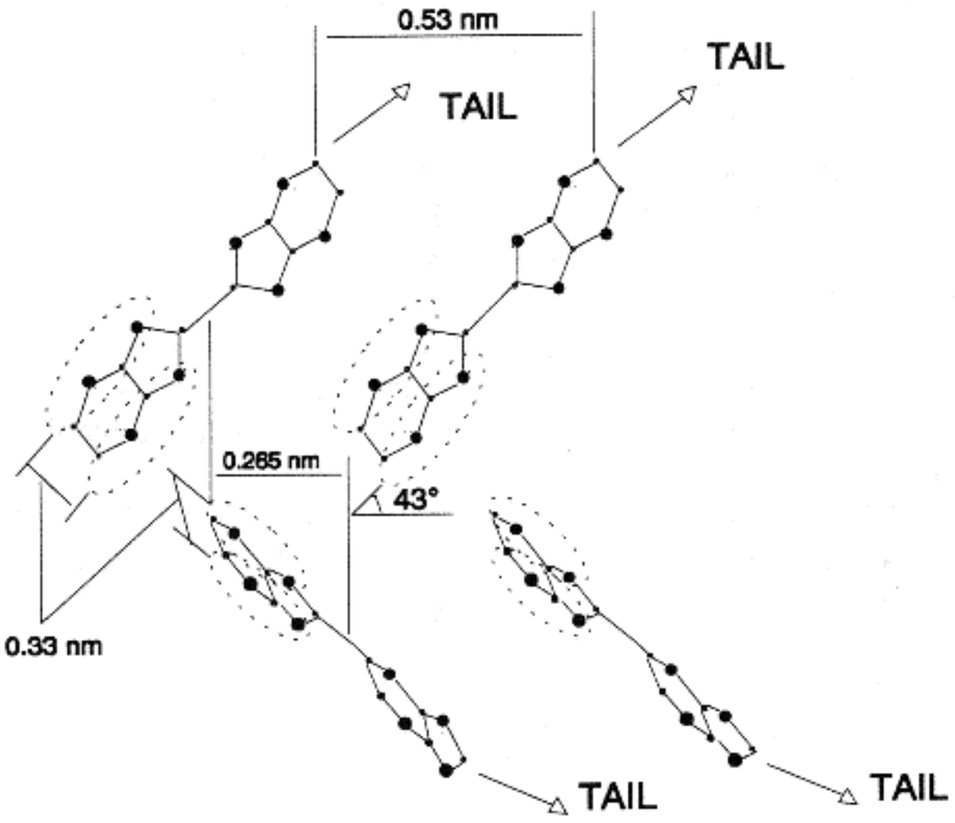

Fig. 6. One possible model of BEDT-TTF group packing.

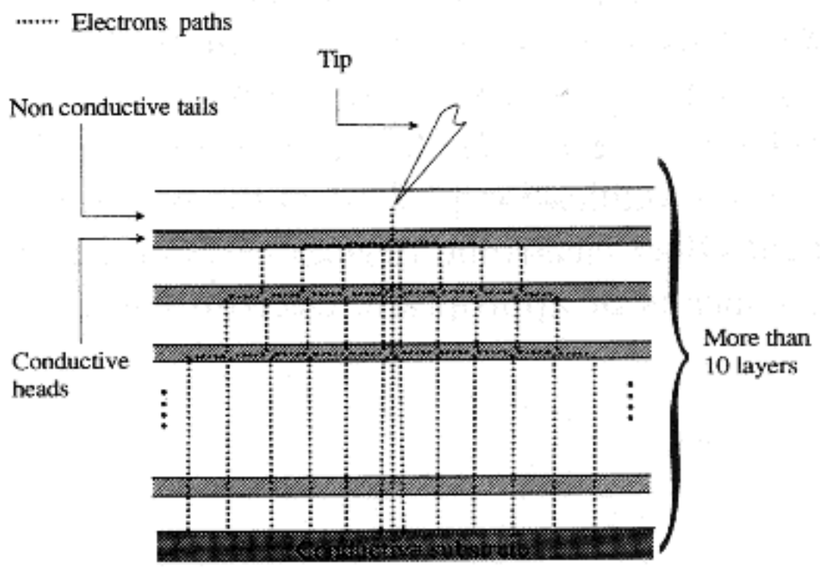

Fig. 7. Paths of electrons inside LB CTS films.

mean tunnelling current was varied with consequent changes in the tunnelling distance.

Finally it is useful here to show a possible scheme of the paths followed by electrons of the tunnelling current from the tip to the substrate. Ideally, this scheme, because of the film anisotropy, has to be something similar to that shown in Fig. 7 assuming a radial symmetry along the central vertical axis.

According to such a scheme the passage from one conductive monolayer to the other should occur via the tunnel effect. If it were so, the effective tunnel voltage (*i.e.* the voltage between the tip and the upper monolayer) should depend on the number of monolayers because of the non-negligible drop of voltage on every monolayer, and a correlation between the number of monolayers and the image quality should exist. However, such a correlation has not been observed. It can be reasonably assumed that typical LB film defects (pinholes, grain boundaries, subphase ions) are located between different monolayers favouring vertical conduction and reducing the voltage drop through film.

4. Conclusions

Images of LB conductive charge-transfer salt films of C_{16}-BEDT-TTF have been obtained by STM on an atomic scale showing a monoclinic or triclinic unit cell of the crystalline lattice. Unit cell parameters and spacings have been found to be consistent with electron diffraction data. The high reproducibility of the acquired images allowed the calculation of the unit-cell parameters (a, b and γ). Several types of errors occurring in the data acquisition and elaboration have been discussed and corrected when possible.

The interest in these films is growing owing to the possibility of using them for a new generation of nanoelectronic devices. The possibility of using STM in a field emission mode for the definition of nanometric structures on a semiconductor and a superconductor substrate has already been proved [24–26]. Our future work will focus on fusing both techniques to build electronic devices based on ordered monolayers of charge-transfer salts deposited on an insulating substrate. The additional property of such films becoming insulators under local electron radiation without substantial structural modification [27] offers the possibility of creating field effect electronic devices of nanometric dimensions by means of appropriate electron emitters.

Acknowledgment

We thank Dr. A.Barraud for the helpful comments and suggestions.

References

1 A. Ulman, *Ultrathin Organic Films*, Academic Press, San Diego, CA, 1991, p. 339.
2 G. Binnig and H. Rohrer, *Helv. Phys. Acta*, *55* (1982) 726–735.
3 G. Binnig, C. F. Quate and Ch. Gerber, *Phys. Rev. Lett.*, *56* (1986) 930–933.
4 H. Fuchs, W. Schrepp and H. Rohrer, *Surf. Sci.*, *182* (1987) 391–393.
5 D. P. E. Smith, A. Bryant, C. F. Quate, J. P. Rabe, Ch. Gerber and J. D. Swalen, *Proc. Natl. Acad. Sci. USA*, *84* (1987) 969–972.
6 C. A. Lang, J. K. H. Hörber, T. W. Hänsch, W. M. Heckl and H., Möhwald, *J. Vac. Sci. Technol. A*, *6* (1988) 368–370.
7 H. Fuchs, *Physica Scripta*, *38* (1988) 264–268.
8 J. H. Coombs, J. B. Pethica and M. E. Welland, *Thin Solid Films*, *159* (1988) 293–299.
9 H. G. Braun, H. Fuchs and W. Schrepp, *Thin Solid Films*, *159* (1988) 301.
10 R. Kuroda, E. Kishi, A. Yamano, K. Hatanaka, H. Matsuda, K. Eguchi and T. Nakagiri, *J. Vac. Sci. Technol. B*, *9* (1991) 1180.
11 R. Fainchtein and J. C. Murphy, *J. Vac. Sci. Technol. B*, *9* (2) (1991) 1013.
12 M. Yoshimura, N. Ara, M. Kageshima, R. Shiota, A. Kawazu *et al.*, *Surf. Sci.*, *242* (1991) 18.
13 S. Magonov, J. Schuchhardt, S. Kempf, E. Keller and H. J. Cantow, *Synth. Met.*, *40* (1991) 59.
14 S. N. Magonov, G. Bar, E. Keller, E. B. Yagubskii and H. J. Cantow, *Synth. Met.*, *40* (1991) 247.
15 S. N. Magonov, S. Kempf, J. Schuchhardt, G. Bar, W. Gronski and H. J. Cantow, *Synth. Met.*, *41–43* (1991) 1815.
16 A. Ruaudel-Teixier, M. Vandevyver and A. Barraud, *Mol. Cryst. Liq. Cryst.*, *120* (1985) 319.
17 A. S. Dhindsa, M. R. Bryce, J. P. Lloyd and M. C. Petty, *Thin Solid Films*, *165* (1988) 197.
18 C. Pearson, A. S. Dhindsa, M. R. Bryce and M. C. Petty, *Synth. Met.*, *31* (1989) 275.
19 V. I. Troitsky, T. S. Berzina, P. S. Sotnikov, T. V. Ujinova and O. Ya. Neylands, *Thin Solid Films*, *187* (1990) 337.
20 T. S. Berzina, V. I. Troitsky, E. Stussi, M. Mulè and D. de Rossi, *Synth. Met.*, *60* (1993) 111.
22 P. Batra and S. Ciraci, *J. Vac. Sci. Technol. A*, *6* (1988) 313.
23 S. V. Ayrapetiants, T. S. Berzina, S. A. Shikin and V. I. Troitsky, *Thin Solid Films*, *210/211* (1992) 261.
24 M. A. McCord and R. F. W. Pease, *J. Vac. Sci. Technol. B*, *3* (1985) 1989.
25 M. Ringger, H. R. Hidber, R. Schlögl, P. Oelhafen and H. J. Güntherodt, *Appl. Phys. Lett.*, *46* (1985) 832.
26 M. A. McCord and R. F. W. Pease, *J. Vac. Sci. Technol. B*, *4* (1986) 86.
27 T. S. Berzina, S. L. Vorobyova, V. I. Troitsky, V. Yu. Khodorkovsky and O. Ya. Neilands, *Thin Solid Films*, *210/211* (1992) 317.